Arabian Journal of Geosciences (2023) 16:617
https://doi.org/10.1007/s12517-023-11725-2

ORIGINAL PAPER

Shallow-water hyperpycnites in the Asara Shale, Karaj Formation, Eocene, Iran

Mohammad Malekzadeh[1] · Maahboubeh Hosseini-Barzi[1] · Abbas Sadeghi[1] · Carlos Zavala[2,3]

Received: 27 June 2023 / Accepted: 9 October 2023 / Published online: 25 October 2023

Abstract

The depositional environment of Asara Shale is discussed in this paper through the detailed analysis of outcrops from the Alborz Basin, NW of Tehran, Iran. The Asara Shale is composed of fine-grained clastic and carbonate (marlstone) strata interbedded with tuff levels. Sedimentary structures include mm- to cm-scale parallel and cross laminations, basal gutter cast, *Thalassinoides* burrows, bioturbation, clastic/biogenic particle alignment, and normal-size grading.

Facies analysis suggests an accumulation dominated by periodic flood energy fluctuations, here related to shallow-marine hyperpycnal discharges. Based on the sedimentary architecture and analysis of the facies associations, five main sedimentary facies have been defined in these outcrops, corresponding to S1, S2, S3, S4, and MM. Suspended-load-dominated facies (Facies S) are related to sedimentation from weak turbulent suspensions and consist of massive sandstones (S1), parallel and low-angle-laminated sandstones (S2), ripple-marked sandstones (S3), parallel-laminated/massive siltstones and mudstones (S4), and microbial mats (MM).

Ratios of redox-sensitive elements indicate that the Asara Shale accumulated in an oxygenated depositional environment. This environment is associated with the presence of parallel-crested ripple marks, microbial-induced sedimentary structures (i.e., wrinkle structures), plant fragments, and surface-grazing gastropods. Based on a variety of sedimentary textures and structures, a shallow-water depositional environment is proposed.

This study offers new insights into the depositional environment of Asara Shale. Due to the oxic character of this sedimentary basin, and the lack of significant organic matter, it is interpreted that the Asara Shale is not a potential hydrocarbon source for the future explorations.

Keywords Alborz Basin · Asara Shale · Hyperpycnal flow · Karaj Formation · Sedimentary processes · Shallow marine setting

Introduction

Much research has focused on the origin of organic-rich shale and mudstone successions because of their roles as both source rocks and unconventional reservoirs. This study offers the first comprehensive study of the depositional environment of the Asara Shale Member of Karaj Formation in the northeast of Tehran, Iran.

The Asara Shale Member belongs to the Middle to Upper Eocene clastic succession of the Karaj Formation, interpreted as being deposited during the tectonic break-up of Mesozoic platforms of the northern Iran region of Pangea (Allen et al. 2003). The Asara Shale accumulated contemporaneously with Middle Eocene submarine volcanic eruptions that generated a thick succession of pyroclastic deposits. The petrographic features of clastic rocks

Responsible Editor: Attila Ciner

✉ Mohammad Malekzadeh
Mo7ammadmalekzadeh@gmail.com

[1] Sedimentary Basins and Petroleum Department, Faculty of Earth Sciences, Shahid Beheshti University, Tehran 1983963113, Iran

[2] Departamento de Geología, Universidad Nacional del Sur, San Juan 670, 8000 Bahía Blanca, Argentina

[3] GCS Argentina SRL, Molina Campos 150, 8000 Bahía Blanca, Argentina

allow for the evaluation of various aspects related to their mode of formation, reservoir characteristics, diagenetic processes, lithofacies types, and sedimentary environments (Yu et al. 2018). The presence of gypsum lenses in the uppermost part of the volcaniclastic succession from the Alborz Mountains, as well as intense folding of tuffs in the Alamout region of the Alborz Range, suggested to Asiabanha and Foden (2012) that the volcano-sedimentary trough was uplifted and deformed by compressive forces during Late Eocene time.

Most details of the depositional environment of the Karaj Formation are still unsolved. Amini and Bolourian (2005), for example, suggested that the Karaj Formation, especially the Asara Shale, accumulated in a submarine fan environment in a broadly deep-water environment. On the other hand, Malekzadeh (2016), based on an analysis of sedimentary structures, faunal evidence, and paleoredox data, proposed for the Karaj Formation an accumulation in shallow-water conditions.

Geological setting

Karaj Formation and Asara Shale in the Central Alborz range

The study area is located in the central Alborz, northeast of Tehran, Iran, between longitude 35° 45′ and 35° 86′ E and latitude 51° 30′ to 51° 47′ N (Fig. 1).

Crustal extension during the Eocene (55–34 Ma) resulted in subsidence of the southern Alborz area, whereas the northern Alborz likely remained a geographic high. Extension was paired with widespread submarine volcanism and deposition of a thick sequence of volcanic and volcaniclastic sediment in the southern Alborz area (Rezaeian 2008). Exposures in the central Alborz display marine and continental successions interpreted as being accumulated from Precambrian through Cenozoic time in successive basins of diverse structural affinities. Deposition of the studied volcanogenic deposits is attributed to the Assyntic orogeny focused along Eurasia and Gondwana that resulted in closure of the Proto-Tethys or Tethys Oceans (Lasemi 2001). Paleozoic mafic volcanic and ophiolitic rocks in the northern Alborz are remnants of the Paleo-Tethys along the northern margin of the Alborz Range.

The Mesozoic sedimentary history of the southern Alborz begins with shallow-water Triassic deposits overlain by a thick sequence of continental/continental-marine facies of the Shemshak Formation and its equivalents (Nazari et al. 2003). Cenozoic deposits in the Alborz Range, especially along its central southern margin, consist mainly of Paleogene volcano-sedimentary successions (Karaj Formation) deposited in a number of transtensional basins related to subduction of Neo-Tethys oceanic crust in a back-arc basin. Subduction was associated with the formation of the Alborz magmatic arc in the southern and western wedges (Nazari 2000).

The Eocene marine volcano-sedimentary sequence (Karaj Formation) is 3320 m thick in its type area (Karaj Valley, central Alborz Mountains) and consists of five members (Dedual 1967) (Fig. 2a). The lower, middle, and upper members are mainly shale units, whereas the second and fourth members consist of green tuffites (Abbassi and Lockley 2004) (Fig. 2a). Overall, the Karaj Formation in the study area comprises a 541-m-thick succession of interbedded clastic tuffs and tuffs (about 132 m), marly mudrocks to marlstones (about 291 m), interbedded tuffaceous marlstones and mudrocks (about 53 m), and clayey marlstones interbedded with thin tuff layers (about 65 m) (Malekzadeh 2016; Fig. 3). The Asara Shale is the third member. It overlies unconformably the Middle tuff and underlies conformably the Upper tuff members (Fig. 2b, c). The Asara Shale is dominated by interbedded marly shale, carbonate, and tuff (Malekzadeh et al. 2020), and with some interbedded pale yellow volcaniclastic layers, 2–43 cm in thickness (Malekzadeh 2016). Following Malekzadeh and Wetzel (2020, see their Fig. 11), the sediments constituting the Asara Shale were delivered from a magmatic arc, and transported by rivers across a nearly filled to overfilled back-arc basin representing a wide plain where the bedload was deposited.

Generally, the Middle Eocene in Iran was a time of active tectonism and magmatism. Walker and Fattahi (2011) found evidence of climatically driven landscape changes across Iran around 10 ka, indicating aridification. Ataabadi and William (2000) discovered mammal footprints in volcanic deposits in eastern Iran, showing that the area was inhabited by ungulates and carnivores at that time. Morley et al. (2009) studied the Central Basin, a region between the Zagros and Alborz Mountains, finding that it underwent extension and transtension in the early-middle Miocene, accumulating up to 5 km of sediment. The Middle Eocene in the Zagros Mountains of Iran was a time of major tectonic and depositional changes. According to Modarres et al. (2018), the Middle Eocene Shahbazan Formation in the Zagros Basin consisted of thick carbonate deposits that were pervasively dolomitized. Maleki et al. (2021) stated that the Middle Eocene was also a time of major source rock deposition, Pabdeh, and underlying Kazhdumi Formations in Zagros.

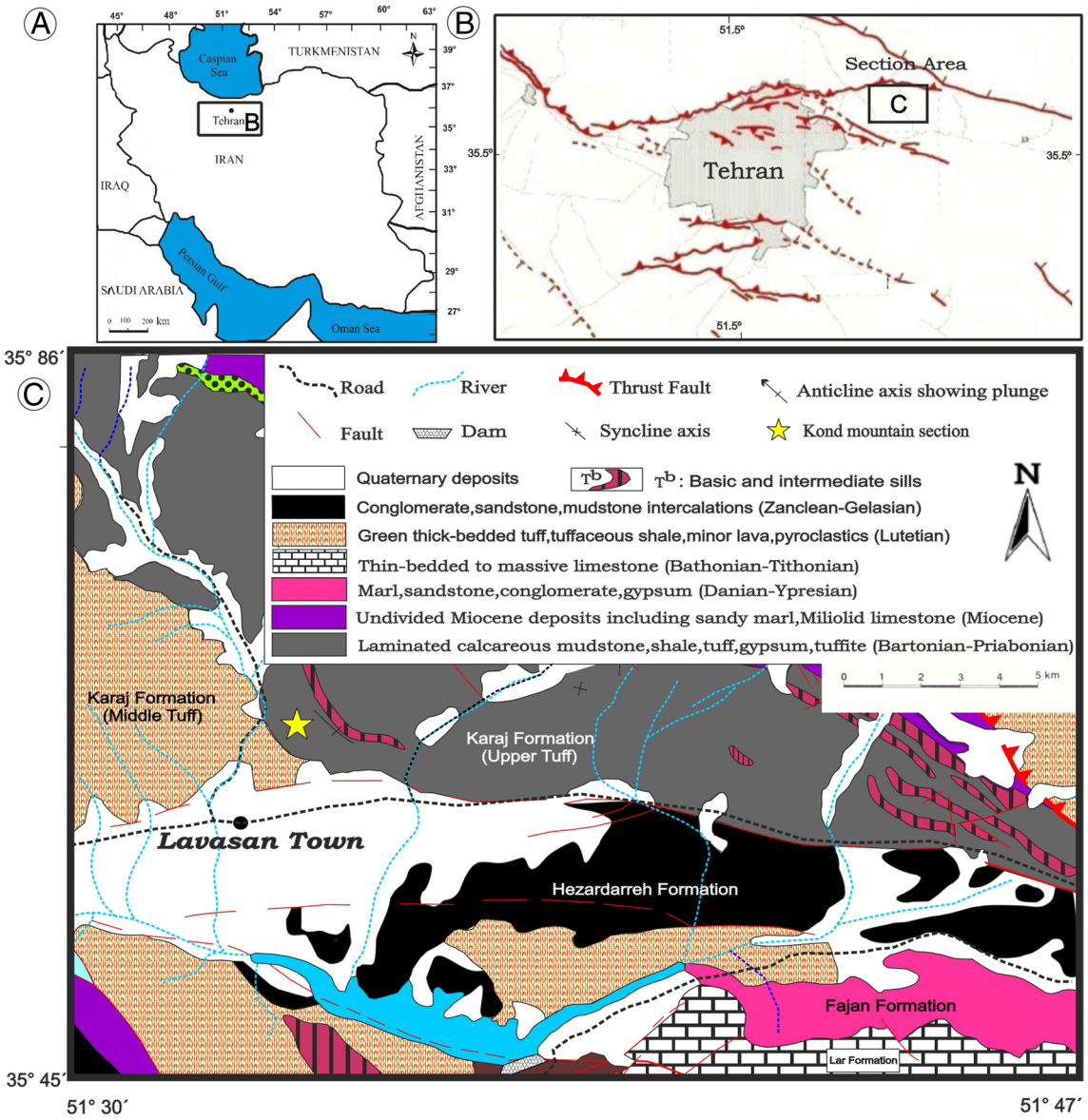

Fig. 1 **A** Map of Iran. The inset represents the area shown in B. **B** Map of the Tehran area displaying selected structural elements (after Nazari 2000). The inset refers to the study area map shown in C. **C** Simplified geological map of the study area (modified after Malekzadeh et al. 2020 and Vahdati Daneshmand 1997)

Methods and materials

This work is based on the detailed analysis of the Kond section, which is located at the northwest of Tehran (Eocene Alborz basin). The studied interval consists of a succession of mudstones and siltstones to fine-grained sandstones with interbedded tuff levels, more than 541 m thick. Lithology and sedimentary structures were described with the help of a hand lens in the field and then completed from rock sample analysis in the laboratory. Rock samples were collected from every lithofacies of the outcrop. Special samples displaying some noticeable sedimentary structures were collected additionally.

Two hundred and fourteen samples of the Asara Shale were recovered from the Kond section for petrographic analysis. Thin sections were made and studied under plane-polarized light (PPL) and cross-polarized light (XPL). Additional information was gathered from scanned photos of samples and thin sections. This allowed for detecting subtle changes in grain size and studying microscopic features. Statistical parameters of textural characteristics, including grain size, sorting, roundness, and compaction, were carried out on thin sections.

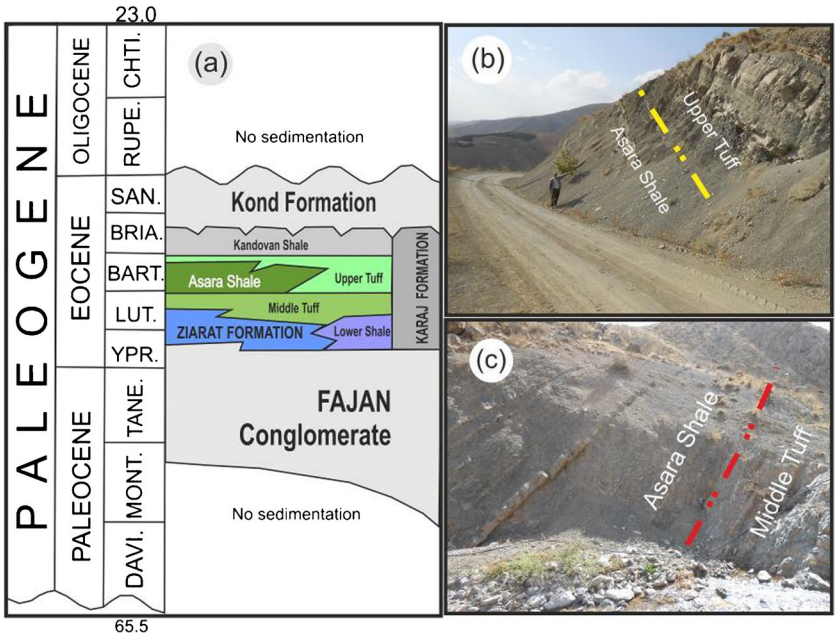

Fig. 2 **a** Generalized stratigraphy of the Paleogene at central Alborz area (modified from Malekzadeh 2016). **b** Conformable contact of the Asara Shale and the upper tuff member of the Karaj Formation in the studied section. Abbreviations: BART. Bartonian, DAVI. (DAN.) Danian, LUT. Lutetian, PRI. Priabonian, MONT.(SEL.) Selandian, THAN. Thanetian, YPR. Ypresian. **c** Unconformable contact of the Asara Shale over the Middle Tuff at the studied section

Sample preparation for geochemical analysis began with the elimination of weathered surfaces by chipping, after which samples were cleaned with distilled water. Weathered surfaces and joint calcite veins were avoided. Cleaned samples were powdered in a swing mill to 200 mesh. Twenty samples were selected for elemental analysis by inductively coupled plasma-mass spectrometry (ICP-MS) using a Siemens (model SRS 303) and standard curves based on International Rock Standards at the laboratory of the Geological Survey of Iran. In the studied deposits, facies were identified based on both field features and laboratory analysis. Facies classification schemes used in this paper are based on those proposed in previous studies (Lash 2016; Xian et al. 2018; Zavala and Pan 2018; Zavala 2020; Zavala et al. 2011).

Results and interpretation

In order to make the results, we applied the petrography, facies classifications, and Redox conditions to the interpretation of the strata of Asara Shale of Karaj Formation.

Petrography

The Asara Shale mainly consists of mudstones with interbedded fine-grained tuffaceous sandstones and tuff beds. Thin section analysis of Asara Shale samples reveals the presence of microbial mats, foraminifera, bioturbation, and other evidence of organic activity. Volcaniclastic deposits in this area consist of sandy crystal lithic to sandy lithic crystal tuff with less than 30% of silt- to fine-sand sized clastic particles (summarized in Table 1). Diagenetic processes in these beds include physical compaction, fracturing, calcite, and chlorite cementation (Malekzadeh 2016).

The tuffaceous layers were divided into lithofacies based on bed thickness, lithology, texture, and sedimentary structures (Haaland et al. 2000). No scientific research has already been performed on the sedimentology of the Karaj Formation and Asara Shale, but partial studies have suggested that Asara Shale is composed of calcareous shale, tuffaceous sandstone, glass tuff, and some marlstone layers. The textural analysis shows that tuffaceous sandstones are medium- to fine-grained, made of subangular to subrounded and poorly sorted particles.

The main grain types found in the tuffs and tuffaceous sandstones are as follows:

Quartz

Quartz grains remain are entirely of monocrystalline (Qm), with no inclusions and with uniform extinction. Along with the presence of potassium feldspar, this suggests provenance from felsic volcanic ashes. Quartz grains are angular and range from silt to sand in size, from 0.5 to 1 mm (Fig. 4a, b).

Feldspar grains

Feldspar grains are subangular and partially altered (Fig. 4b, c). They consist of plagioclase crystals with polysinthetic twinning and zoning and of some orthoclase. Grain rounding

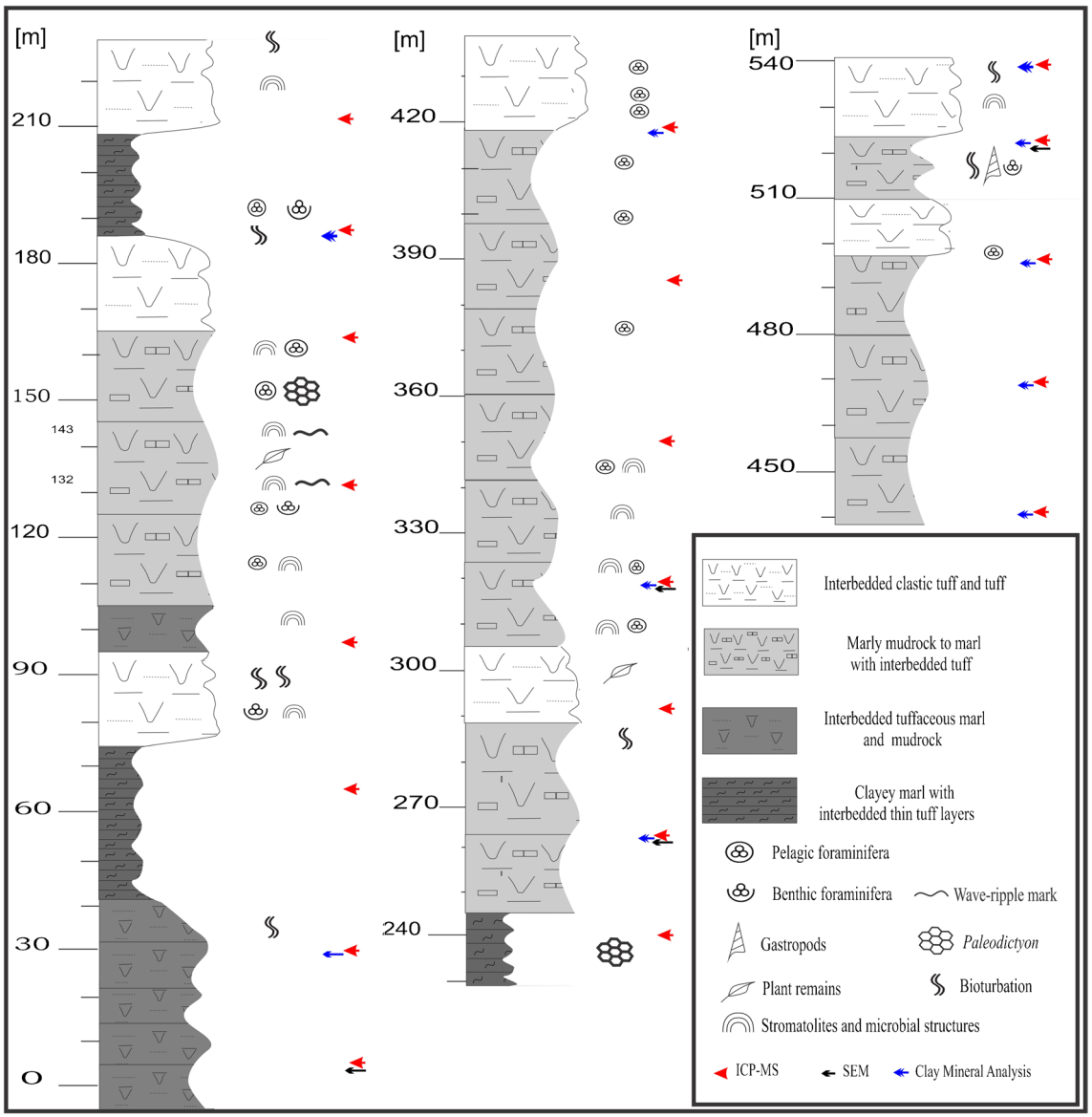

Fig. 3 Lithologic log of the Asara Shale from the Kond section showing lithofacies types, body- and trace-fossil distribution, and sample location. The right edge of the log represents the resistance to weathering (erosion) as seen in field observations (modified from Malekzadeh and Wetzel 2020)

is very low suggesting a short transport from the source area. Some of the feldspar grains are corroded by carbonate cement.

Lithic fragments

A variety of rock fragments have been observed in thin sections, including fragments of sedimentary rock (Ls) and volcanic igneous rock (Lv). Rock fragments and corresponding feldspar particles are the main particles; the frequencies of other particles are not high, so the abundance of rock fragments (flint, sediment) is greater than that of feldspar grains. These volcanic fragments are hyaline porphyritic microlithic, interseptal, and fine-grained felsic textures (Fig. 4c, d).

Fragments indicate that at the time of the deposition of Asara Shale, volcanic rocks were eroded and deposited. Furthermore, thin section analysis reveals that grains detectable under (PPL and XPL) microscope are mostly angular and poorly sorted these particles illustrate a little grinding through the transportation process. In other words, this subject suggests an accumulation in

Table 1 Summarized petrography and description of selected samples from the Asara Shale

Representative samples	Location (m)	Lithology	Mineral composition of tuff interbedded	Microbial structures and Skeletal allochem
AS 11	33	Interbedded tuffaceous marl and mudrock	5% quartz, 60% plagioclase, 1% biotite,34% clay matrix	–-
AS 71	213	Interbedded clastic tuff and tuff (sandstones)	80% plagioclase, 10% biotite	Bioturbation, benthic foraminifera, pelagic foraminifera, microbial mats, plant remains
AS 81	243	Clay marl with interbedded thin tuff layers	–-	Shallow paleodictyon, bioturbation, benthic foraminifera, pelagic foraminifera
AS 93	291	Marly mudrock to marl with interbedded tuff	10% plagioclase, 15% rock fragments	Gastropoda, Shallow paleodictyon, bioturbation, bentic foraminifera, pelagic foraminifera, microbial mats, plant remains

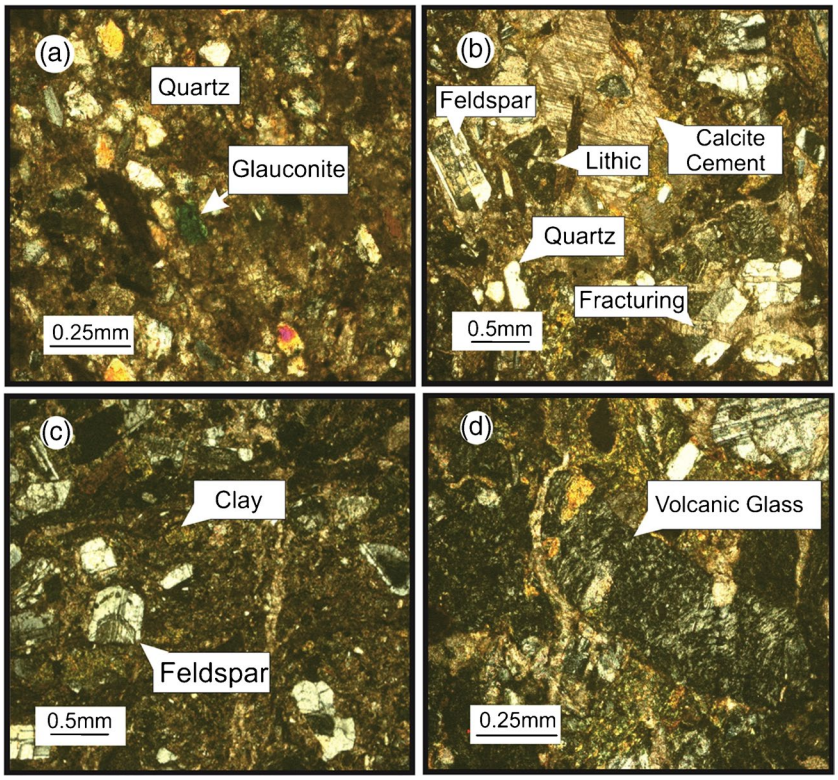

Fig. 4 Selected photomicrographs, viewed under crossed-polarized light. **a** Subangular-angular quartz grains with glauconite. **b** Lithic grain with lamellar-twinned plagioclase feldspar with calcite cement. **c** Plagioclase feldspar with zoning and clay after volcanic glass alteration. **d** Volcanic glass grain

a low-energy setting with minimal sediment reworking. The petrography and structural features of Asara Shale deposits are summarized in Table 1. Petrographic features and sedimentary structures of Asara Shale deposits are summarized in Table 1.

Facies classification

The Asara Shale is dominantly composed of mudstones with interbedded fine-grained sandstone levels. The detailed analysis of the clastic section allows the recognition of five sedimentary facies, termed as S1, S2, S3, S4, and MM. This facies classification is partially based on the genetic facies scheme proposed by Zavala et al. (2011).

Facies S1 (massive sandstones)

Description This facies is characterized by light and green-brown, fine to very fine-grained massive and poorly sorted sandstones. Divisions of this facies display an erosional base and often overlie the massive siltstones and mudstones (Fig. 5A, C) capping the underlying bed (Fig. 5). They are usually less than 4 cm thick, forming the

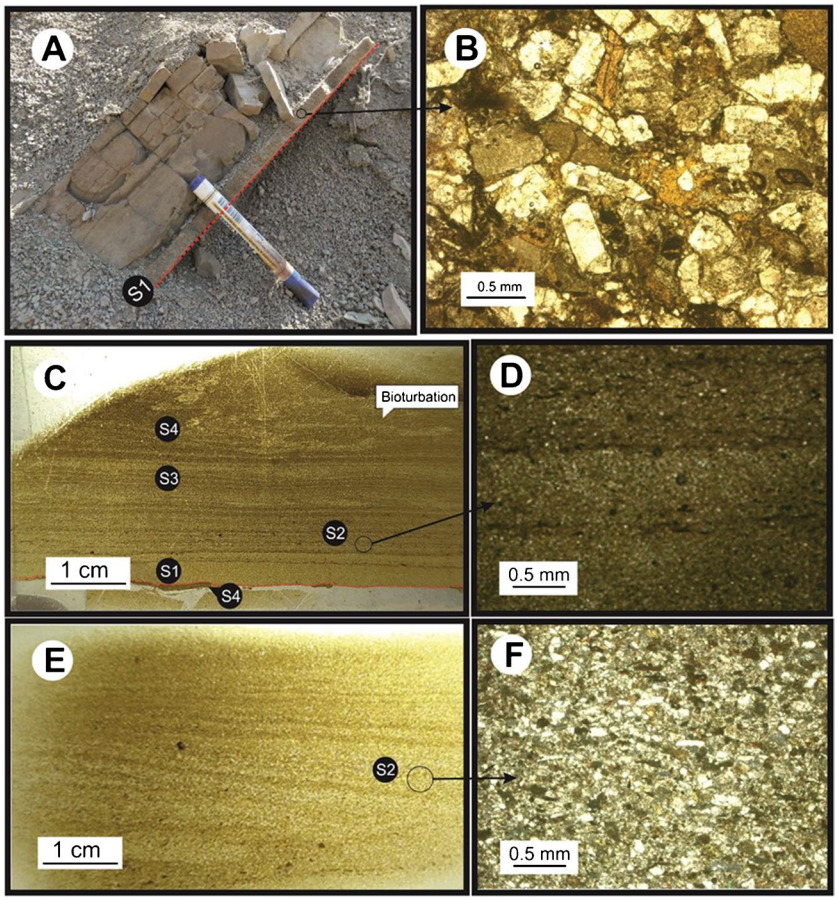

Fig. 5 Outcrop and thin section photos of Facies S1 and S2. **A**, **B** Outcrop and thin section of Facies S1 over a sharp (erosional) contact (Red line). **C**, **D** Scanned and thin section photos of planar-laminated sandstones (Facies S2). **E**, **F** Scanned thin section photo of Facies S2 (S2h), showing low-angle cross-bedded sandstones, composed of graded silt/clay couplets with fading ripples in the lower half, and siltstone with parallel laminae grading to clay, in the upper half

base of the thickest beds of sandstones (Fig. 8A). In turn, facies S1 divisions gradually evolve upwards into laminated sandstones (Facies S2), which are finally overlain by massive siltstones and mudstones (Facies S4) (Fig. 8). S1 deposits are deposited on some erosional surfaces, and they usually are exposed as sandstone tuffs in the field (Fig. 5A). Some intervals/divisions of Facies S1 show a coarsening-upward trend. Field observations reveal that this facies commonly display flute/tool casts (Fig. 9b-d) (e.g., Malekzadeh 2016).

Table 2 Summary of features for the identified facies in the Asara Shale

Facies	S1	S2	S3	S4	MM (microbial mats)
Description items					
Color	Light brown to green-brown	Light brown	Light brown	Gray	Light brown to light green
Laminae thickness	< 4 cm	1 to 2 cm	< 2 cm	1 to 3 cm	< 2 cm
Grain size	Fine to very fine-grained sand	Fine to very fine-grained sand	Fine sand to silt	Silt to clay size	Fine to very fine-grained sand
Upper and lower contacts	Erosional	Erosional to gradational	Sharp to gradational	Sharp to gradational	Erosional
Composition (petrography)	Rock fragments, quartz, plagioclase, biotite, clay minerals	Foraminiferal fragments, detrital quartz, shell fragment	Very fine silt to clay and organic matter	Plant remains	Organic matter, quartz, plagioclase, biotite, clay minerals
Sedimentary structures	Flute/tool casts	Horizontal to subparallel lamination	Ripple and low angle lamination	Horizontal lamination	Lamination
Depositional processes	Hyperpycnal flows	Hyperpycnal flows	Hyperpycnal flows	Hyperpycnal flows	Microbial processes

Interpretation These deposits are comparable to facies S1 of Zavala et al. (2011). The origin of the massive sandstone divisions is related to progressive bed aggradation due to direct suspension sedimentation from waning sediment-laden turbulent flows with high fallout rates (> 0.44 mm/s; Sumner et al. 2008; Dou et al. 2019). The erosional base of this facies probably indicates high-velocity turbulent flows (Table 2).

Facies S2 (planar- and low-angle-laminated sandstones)

Description This facies is composed of fine- and very fine-grained sandstones with parallel or low-angle lamination. Individual laminae, visible in hand specimens and thin sections, are of millimeter to centimeter-scale (Fig. 5C, D). Examples of this facies are composed of planar to wavy laminae. Low-angle cross-bedded sandstones (subfacies S2h) comprise sets of millimeter- to centimeter-scale low-angle cross laminae (Fig. 8C, D). Facies S2 always overlies Facies S1 and is often overlain by sandstones with climbing ripples of Facies S3, with a fining-upward trend (Figs. 5 and 8).

Interpretation This facies is comparable to Facies S2 of Zavala et al. (2011). It is interpreted to result from the fallout of suspended sediment load in the near-bed traction carpets or laminar sheared layers during a flood event (Dou et al. 2019).

The majority of samples show lamina undulations that Zavala et al. (2011) related to the existence of an oscillatory component of the overlying flow. Usually, the amount of suspended load and fallout rates (Sumner et al. 2008) results in variations in the thickness of individual laminae during this process. As it can be seen, the upward thinning of laminae indicates a decreasing suspended load and lower fallout rates from the turbulent suspension. The lateral transition from parallel lamination to climbing ripples suggests a common origin for these structures related to traction-plus-fallout processes (Middleton 1965; Zavala and Pan 2018). The low-angle cross-stratification of Facies S2h (Fig. 5E, F), like some other turbulent flow facies, represents a high flow velocity under a turbulent flow condition. This sedimentary structure (Facies S2h) is common in shallow-water hyperpycnal systems (Zavala et al. 2011).

Facies S3 (fine-grained sandstone/ siltstone with ripple cross-bedding)

Description This lithofacies is finer than facies F2, being composed of very fine-grained sandstone divisions < 2 cm thick, with some sandy lenses (Fig. 6b, c, f). This facies overlies Facies S2 and commonly evolves horizontally and vertically into Facies S4 (discussed below) at outcrop scale (Fig. 6a).

Interpretation This deposit can be classified as Facies S3 of Zavala et al. (2011). Climbing ripples and cross-laminated sandstone lenses indicate bed form aggradation and migration processes associated with high rates of sedimentary fallout from a sediment-laden turbulent flow (Ashley et al. 1982). They can be related to traction-plus-fallout processes from waning turbulent flows (Dou et al. 2019). The asymmetry in the ripples of Facies S3 indicates combined-flow deposits in shallow-water environments partially affected by bidirectional (oscillatory) flows. As a summary, Facies S3 can be interpreted as deposited after a decline in the flow power (Xian et al. 2018; Zavala et al. 2006).

Facies S4 (planar-laminated siltstone and massive siltstone/ mudstone)

Description This facies consists of greyish siltstones and mudstones which commonly overlie sandstone facies (Fig. 8). Two main subfacies were recognized, namely, the planar-laminated siltstones and the massive siltstone/ mudstones. The thickness of laminated layers ranges from less than 1 cm up to 2 cm. This facies often show subtle internal grain-size variations displaying normal grading or inverse then normal grading (Figs. 6, 7, and 8). In addition, plant remains are commonly found in the massive siltstones (Fig. 9e).

Interpretation Several depositional processes have been proposed for the accumulation of mudstones in marine and lacustrine basins, like hemipelagic sedimentation (O'Brian and Slatt 1990), hyperpycnal (extrabasinal) flows (Mulder et al. 2003; Zavala and Pan 2018), turbidity (intrabasinal) flows (Morris 1971), and shelf storm-related sedimentation (tempestites) (Morton et al. 2007). These processes may operate in the same way and distinction amongst them can be difficult. This facies is similar to Facies S4 of Zavala et al. (2011). The massive facies is interpreted as accumulated by the gravitational collapse of a suspended cloud related to muddy hyperpycnal flows. Muddy hyperpycnal flows are originated by the plunging of sustained sediment-laden turbulent flows with a suspended load mainly composed of a clay-silt fraction (Zavala 2020). Since muddy hyperpycnal flows are dominantly composed of silt–clay fractions, the flow will be attached at the bottom until the final accumulation (Zavala 2020) without experiencing density reversal (lofting). Plant debris, as those found in the massive siltstone/mudstone, are

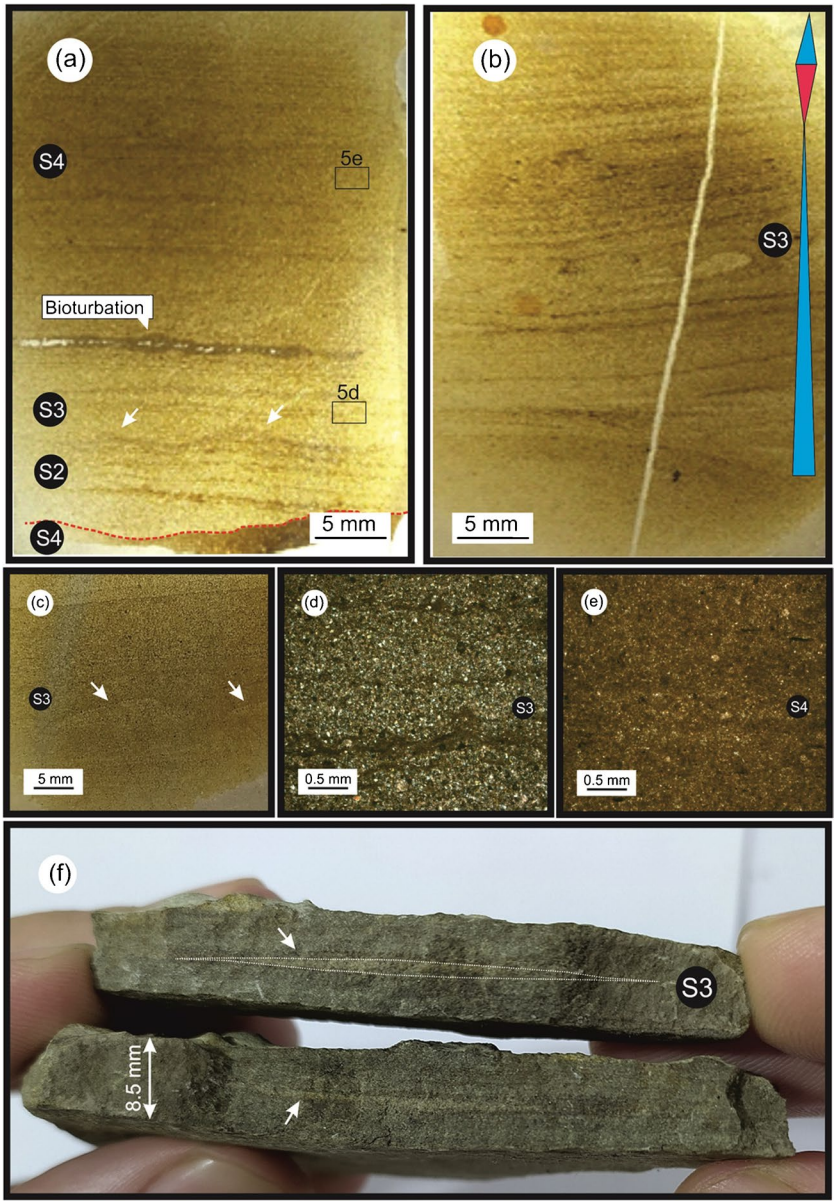

Fig. 6 Scanned, thin section and hand samples of Facies S3 and S4. **a** Scanned and thin section photos of wave ripples sandstone (Facies S3) (white arrows show wave ripples). **b** and **c** Scanned photo of cross-laminated sandstone lenses (Facies S3) (white arrow shows a sandy lens in a silty layer). Note the presence of normal and inverse-then-normal-grading cycles related to waxing-waning cycles. **d** Thin section photo of laminated siltstone (Facies S3) from the scanned sample shown in **a**. **e** Thin section photo of Facies S3 from the scanned sample shown in **a**. **f** Very fine-grained sandy lenses in silt layer. These lenses show distinct low-angle lamination

commonly carried by hyperpycnal flows from land into the subaqueous environment during river flooding (Yoshida et al. 2010). Therefore, the presence of plant remains can be considered evidence of a direct fluvial supply into the basin (Petter and Steel 2006; Zavala et al. 2012). Their presence in Facies S4 suggests that their deposition took place during the final fallout from suspension.

Facies MM (microbial mats)

Description Microbial mats are recorded along the stratigraphic column of Asara Shale in the Kond section at 141 m, 144 m, 153 m, 215 m, and 225 m above the base of the section (Fig. 3). They occur as positive epireliefs recognized on top of tuffaceous sandstone layers (Fig. 10c). In this area, two different modes of appearance of microbial mats have appeared. Flat mats and wrinkled mats sometimes entrained large clasts with higher relief tufted laminations (Fig. 10c). It seems that microbial mats are found on top of sandstone layers, i.e., below the capping muddy divisions and thus within beds. These ridges are rare branches presenting large, winding, short, wavy masses 9–35 cm long and 3–10 mm wide. The upper part of the ridge is semicircular and smooth. These structures typically protrude 1–2 cm above the floor level. Under the microscope, the MM samples in Asara Shale display non-direction-oriented fine quartz and feldspar grains that usually float under

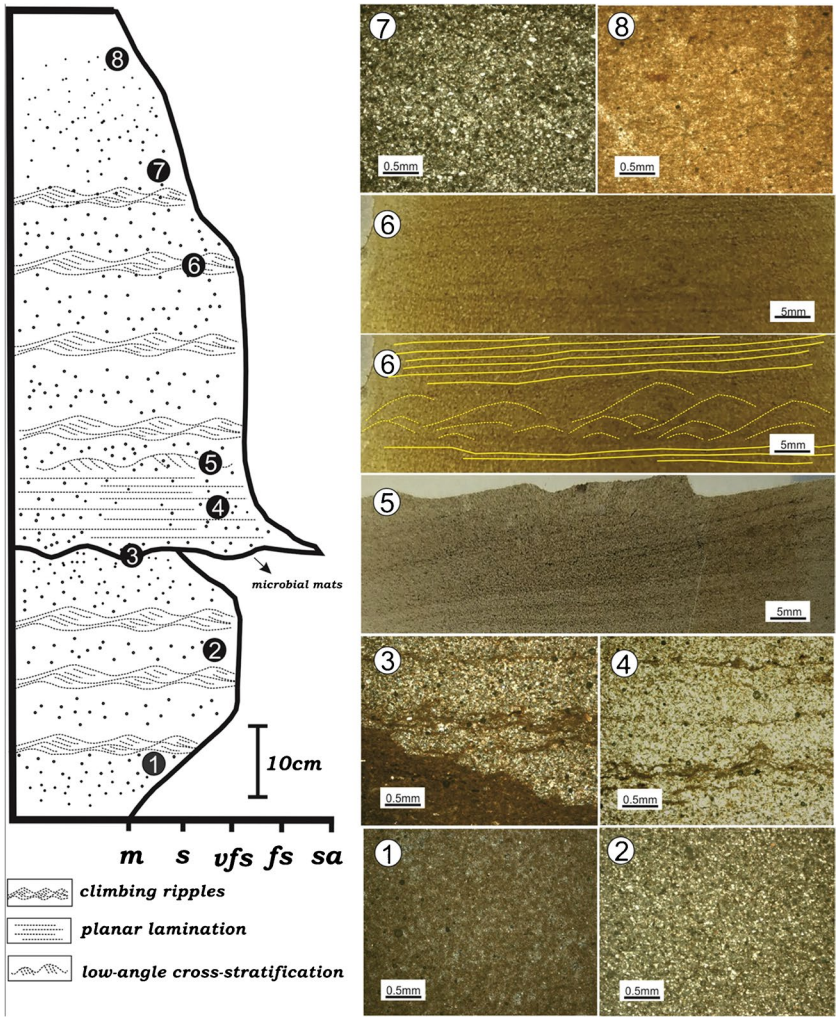

Fig. 7 Conceptual model of bed organization with examples of thin sections from different parts of the profile showing vertical variations in grain size. Note the inverse- then normal vertical trend of the grain size. m, mud; s, silt; vfs, very-fine-grained sand; fs, fine-grained sand; sa, sand. Modified from Dou et al. (2019)

biofilms which are formed by probably a residuum of the microbial mat or weathering of clay minerals) (Fig. 10d). It seems that sand-size particles were trapped by the constantly growing biofilm envelopes causing the forming of some parallel to the bedding planes. The Asara Shale strata reveal the presence of wrinkle structures (Fig. 10a–d) (Hagadorn and Bottjer 1997). The highest abundances of microbial mats were identified in the bottom of tuffaceous strata as erosional contact.

Interpretation Most studies have suggested that microbially induced sedimentary structures (MISS) commonly occur in tidal flat environments with medium turbulence (Noffke 2009; Xing 2010; Zheng et al. 2017). Paleoenvironment, or at least hydraulic conditions, clearly control the diversity and morphology of microbial mats (Hickman-Lewis et al. 2019). These structures are wrinkled sandy surfaces of biological origin that strongly suggest a shallow-marine setting. Additionally, the development of microbial mats requires a low sediment supply (Eriksson et al. 2010). In consequence, the location of microbial mats on top of sandstone beds probably suggests the existence of a short period of non-deposition after the accumulation of sandstone layers and before the fallout of muddy sediments.

Redox conditions

The concentration of redox-sensitive trace metals in sediment is directly or indirectly constrained by the degree of oxygen depletion in the depositional environment (McKay et al. 2007). Twenty mudstone samples of the Asara Shale from the Kond section were taken and prepared for geochemical analysis. Sampling was done in facies S4 intervals, and those samples with the lesser content of calcium carbonate were finally selected and prepared for geochemical analysis (see Table 3) (Fig. 11).

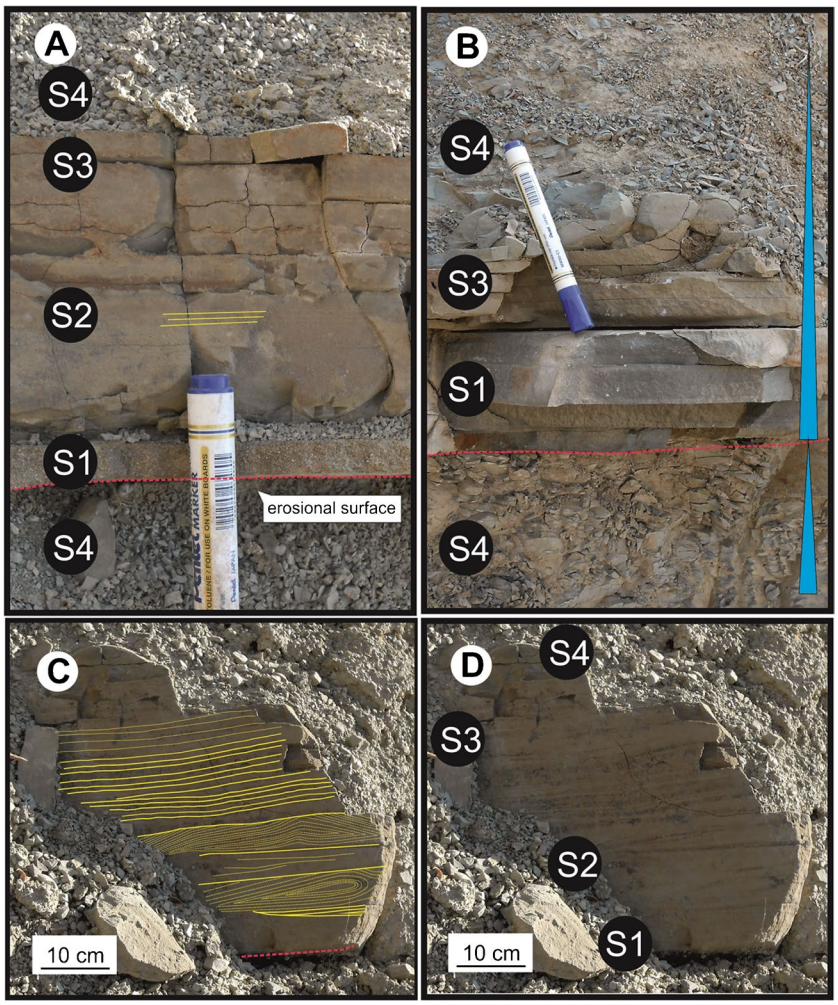

Fig. 8 Photographs of deposits related to suspended-load processes (Facies S). Vertical association of massive muddy siltstone (Facies S4), massive fine-grained sandstones (Facies S1 in **A**), massive very fine-grained sandstones (Facies S1 in **B**); planar-laminated sandstones (Facies S2); low-angle cross-bedding overlying climbing ripples and ripple cross-laminated sandstones (Facies S3 in **C**, **D**); graded muddy facies (Facies S4). The location of this outcrop is shown in Fig. 1

Results of geochemical analysis of the Asara Shale sample suite are presented in Table 3 (Malekzadeh et al. 2020). According to Table 3, the Ni/Co ratio of the Asara Shale samples ranging from 2.48 to 4.40, V/Cr from 1.46 to 2.96, U/Th 0.17 to 0.46, authigenic U – 2.37 to 1.54 (the authigenic uranium = U total—Th/3) reflects an oxic depositional environment (Fig. 12a–c).

Discussion and depositional model

Gravity currents transfer enormous volumes of terrestrial clastic sediments into associated basins (Zavala 2020). Sediment-laden fluvial discharges are land-generated gravity flows capable of plunging on lacustrine and marine waters generating coastal (mainly prodeltaic subenvironments), shallow-water and deep-water hyperpycnites (Mulder et al. 2003; Birgenheier et al. 2017; Steel et al. 2018; Zavala et al. 2021). Lash (2016) tried to explain the relationship between the presence of organic matter in black shale layers and hyperpycnal flows. It seems that Asara Shale deposits are in generally comparable to those described by Lash (2016), and hyperpycnal flows played a significant role in controlling the sedimentation. In the studied section of the Asara Shale, there is ample evidence supporting an accumulation in a shallow-marine depositional system influenced by hyperpycnal flows. Main evidence that support a shallow water origin include the presence of microbially mats (including wrinkle structures), plant fragments (e.g., Buatois and Mangano 2011; Miller 2007; Solanki et al. 2015), and surface-grazing gastropods (e.g., Malekzadeh 2016; Malekzadeh and Wetzel 2020). Wrinkle structures are common in tidal, lagoonal, and continental shelf settings (Noffke 2010). In addition, the occurrence of both illite and chlorite of detrital origin suggests weak weathering of the parent rock in a shallow marine environment (Malekzadeh et al. 2020). Additionally, shallow water

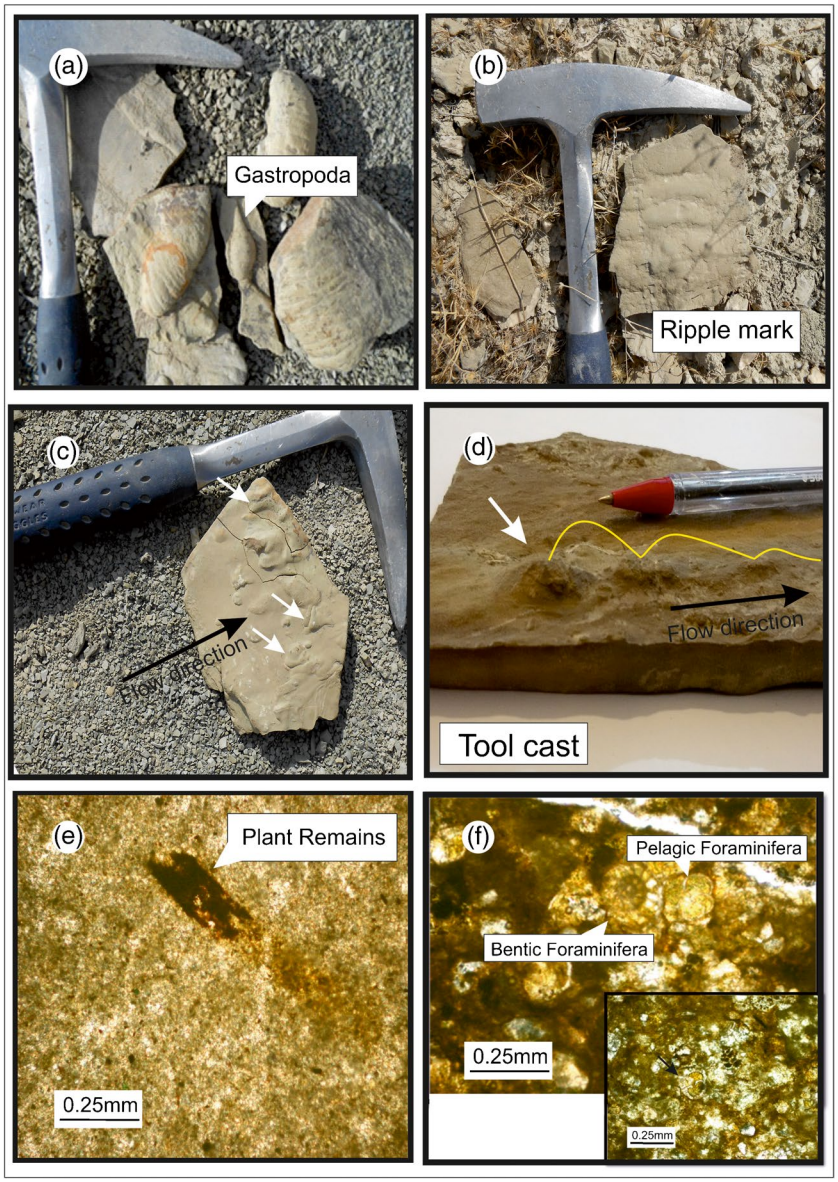

Fig. 9 Fossils and sedimentary structures of the Asara Shale of Karaj Formation: **a** Gastropods in hand samples. **b** Ripple mark in the field. **c** and **d** Flute and tool casts with inferred flow directions indicated by arrows. **e** Plant remains that replaced by iron oxide. **f** Pelagic foraminifera next to benthic foraminifera along with micrite fragments and debris, which indicates a high-energy environment. Pelagic foraminifera smaller than normal size with a thick wall indicated by black arrow

conditions probably affected the paleo-redox conditions, resulting in oxidizing conditions during the accumulation of the Asara Shale.

Hyperpycnal flow deposits in shallow-water settings show different characteristics compared to those developed in a deep waters and other types of sediment gravity flows (SGF) deposits (Dou et al. 2019). Hyperpycnal discharges are often influenced by the energy dissipation process that occurred along the distal delta front. These shallow water wave-modified hyperpycnal flow deposits have been recently considered as part of hyperpycnal littoral deltas by Zavala et al. (2021). In these systems, the deceleration and dilution processes of the hyperpycnal flow are controlled by the relatively flat topography of a shallow marine ramp. These weak hyperpycnal flows are related to the discharge of dirty rivers with relatively low flow density (Plink-Björklund and Steel 2004; Zavala et al. 2021). The paleoclimate of the Eocene Alborz Basin was semiarid (Malekzadeh et al. 2020). Semiarid regions are characterized by mean annual precipitation between 200 and 700 mm (Gallart et al. 2002), often with a stormy character, and clustered in alternating seasons (Nadal-Romero et al. 2018). It seems that under these semiarid conditions the basin suffered common flood events caused by a high discharge variability (Lash 2016; Long 2017). As a result, the presence of loose sediments (volcanic and weathered materials) in source areas could have favored the erosion, loading and transfer of large

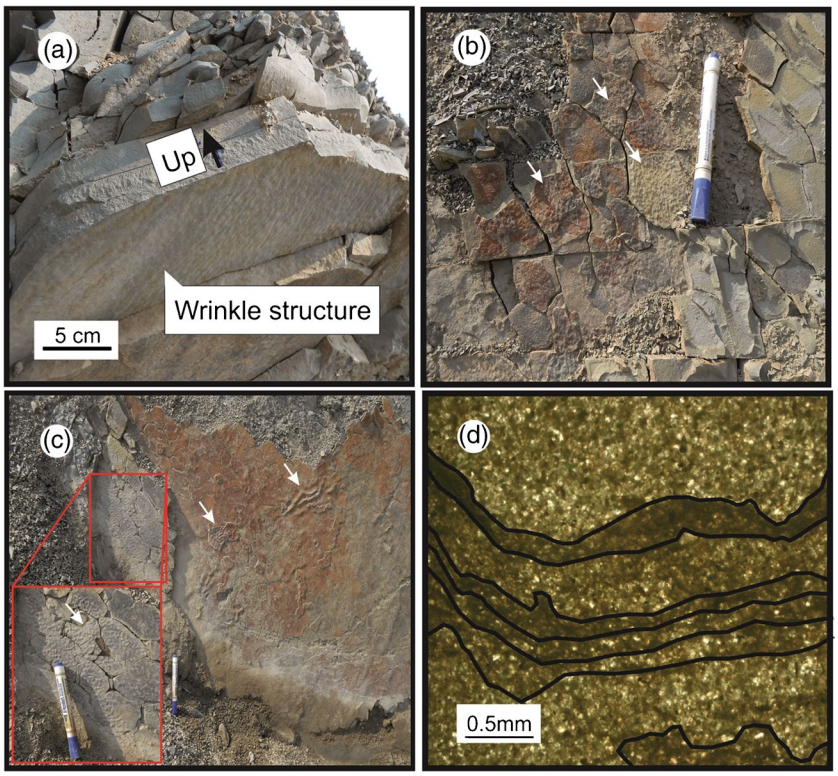

Fig. 10 Photographs of deposits related to microbial mats (Facies MM), and sedimentary structures of the Asara Shale: **a**–**c** outcrop images of microbial mats and wrinkle structures, white arrows show microbial mats and wrinkle structures; **d** microbial mats in thin section

Table 3 Elemental and isotopic data on the Asara Shale, Karaj Formation in the northeast of Tehran, Iran

Field. No	Co (ppm)	Cr (ppm)	Ni (ppm)	Th (ppm)	U (ppm)	V (ppm)	U/Th	Auth U	V/Cr	Ni/Co	V/(V + Ni)
Sh 4	19.44	58.58	55.19	11.49	3.12	118.06	0.27	−0.71	2.02	2.84	0.68
Sh 9	17.76	67.88	69.90	12.90	4.55	115.65	0.35	0.25	1.70	3.94	0.62
Sh 19	15.96	34.26	62.65	11.44	5.08	96.38	0.44	1.27	2.81	3.93	0.61
Sh 35	14.02	68.78	56.67	11.70	4.92	117.23	0.42	1.02	1.70	4.04	0.67
Sh 45	17.83	62.22	52.79	12.23	4.75	120.80	0.39	0.67	1.94	2.96	0.70
Sh 60	21.05	85.99	81.33	13.33	4.36	125.22	0.33	−0.08	1.46	3.86	0.61
Sh 71	22.25	60.49	60.11	12.29	3.93	119.84	0.32	−0.17	1.98	2.70	0.67
Sh 80	17.68	63.28	48.50	12.03	4.27	115.72	0.35	0.26	1.83	2.74	0.70
Sh 96	15.22	62.38	55.76	12.69	4.76	127.56	0.38	0.53	2.05	3.66	0.70
Sh 105	15.25	51.45	62.86	14.98	5.00	98.73	0.33	0.00	1.92	4.12	0.61
Sh 115	20.56	81.90	58.66	11.04	4.85	132.15	0.44	1.17	1.61	2.85	0.69
Sh 125	20.03	63.93	59.95	12.43	3.06	123.08	0.25	−1.08	1.93	2.99	0.67
Sh 136	15.84	77.41	64.63	12.61	5.07	123.83	0.40	0.87	1.60	4.08	0.66
Sh 145	15.83	60.80	43.59	13.83	4.24	123.42	0.31	−0.37	2.03	2.75	0.74
Sh 155	20.99	55.51	92.45	16.24	5.65	118.53	0.35	0.23	2.14	4.40	0.56
Sh 165	18.11	56.66	59.86	14.60	4.22	118.01	0.29	−0.64	2.08	3.31	0.66
Sh 180	25.71	34.04	63.69	11.96	5.52	100.82	0.46	1.54	2.96	2.48	0.61
Sh 195	17.68	60.63	51.45	14.55	4.62	121.31	0.32	−0.23	2.00	2.91	0.70
Sh 205	25.14	77.83	83.31	12.51	5.54	127.92	0.44	1.37	1.64	3.31	0.61
Sh 210	20.19	72.95	71.53	14.52	2.47	124.87	0.17	−2.37	1.71	3.54	0.64
Mean	18.83	62.85	62.74	12.97	4.50	118.45	0.35	0.18			
Median	17.97	62.30	60.03	12.56	4.69	120.32	0.35	0.24			
Standard division	3.21	13.38	12.06	1.39	0.84	9.58	0.07	0.95			

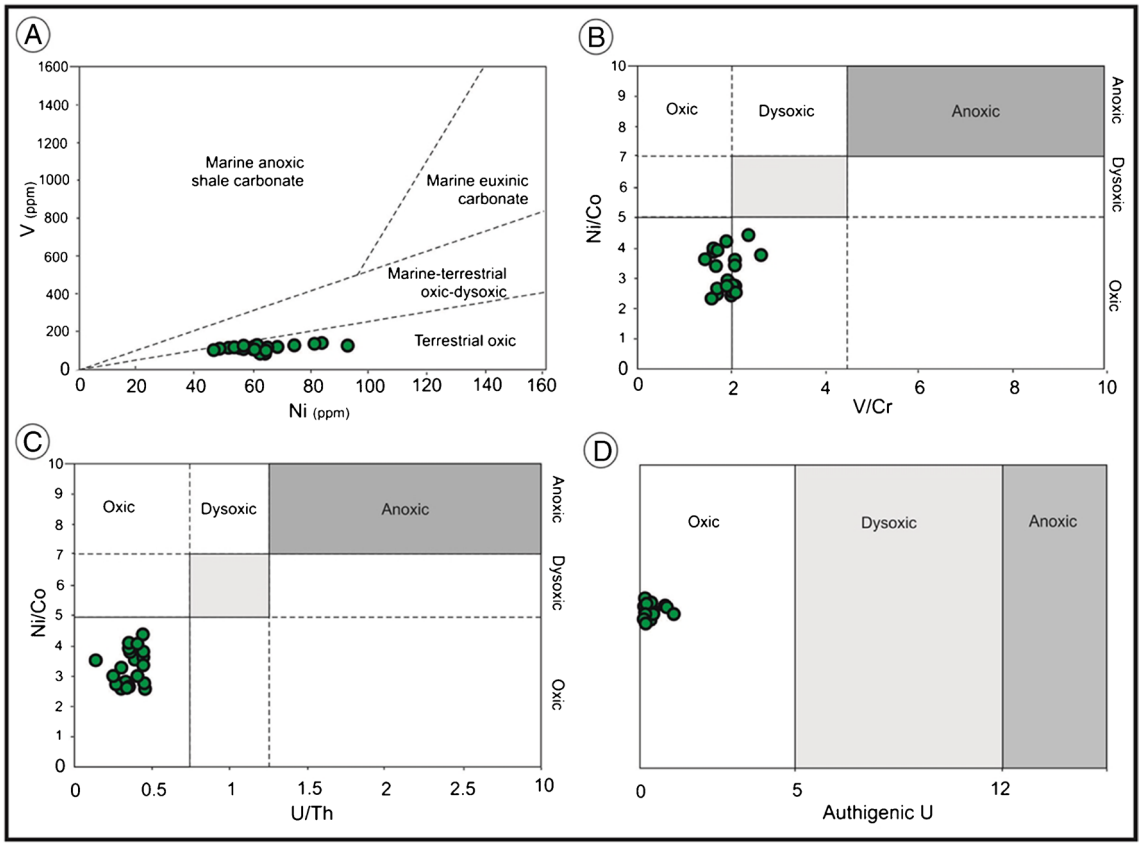

Fig. 11 Cross-plots of trace-element ratios used as paleoredox proxies: **a** V vs Ni; **b** Ni/Co vs V/Cr; **c** Ni/Co vs U/Th; **d** Authigenic U. Diagrams showing redox conditions as oxic, dysoxic, and anoxic environments (the authigenic uranium = U total—Th/3). The ranges for V/Cr and Ni/Co are from Jones and Manning (1994); the ranges for Th/U are from Wignall and Twitchett (1996); and the ranges for dU are from Wignall (1994)

volumes of sediments during relatively intense seasonal rainfall. In other words, the paleoclimate was proper for the development of hyperpycnal flows.

Previous works suggested that the Karaj Formation accumulated in a back-arc basin related to subduction of Neo-Tethys oceanic crust beneath Eurasia (Allen et al. 2003; Asiabanha and Foden 2012; Malekzadeh et al. 2020; Shahidi et al. 2011) (Fig. 12A, B). However, little detailed work has been devoted to elucidating the environment of deposition of the Karaj Formation, especially the Asara Shale.

The Cenozoic deposits in Alborz, especially Karaj Formation (the Asara Shale Member), resulted from a combination of transtensional tectonic and a decrease in water depth in central Alborz basin (Nazari 2000). The Karaj sedimentary basin was affected by multiple volcanic events (Alimi et al. 2010). Volcanism was likely accompanied by the generation of submarine mass flows, including intrabasinal turbidity currents. Such an environment would not have been suitable for a variety of planktonic and even benthic forms with delicate shells, and only those with thick shells can tolerate such a situation (Amini and Bolourian 2005; Bolourian 1992; Lasemi 1992). The presence of thick-walled, small pelagic, and benthic foraminifera (Fig. 9f) provides evidence of turbulent conditions (Amini and Bolourian 2005; Bolourian 1992; Lasemi 1992; Malekzadeh 2016).

It seems that semi-arid climatic conditions and probably stormy heavy rains during the accumulation of the Asara Shale (Malekzadeh et al. 2020) promoted high rates of sediment supply during flood events, causing the generation of hyperpycnal flows. Volcaniclastic debris were sourced by the increasing activity of Eocene submarine volcanos.

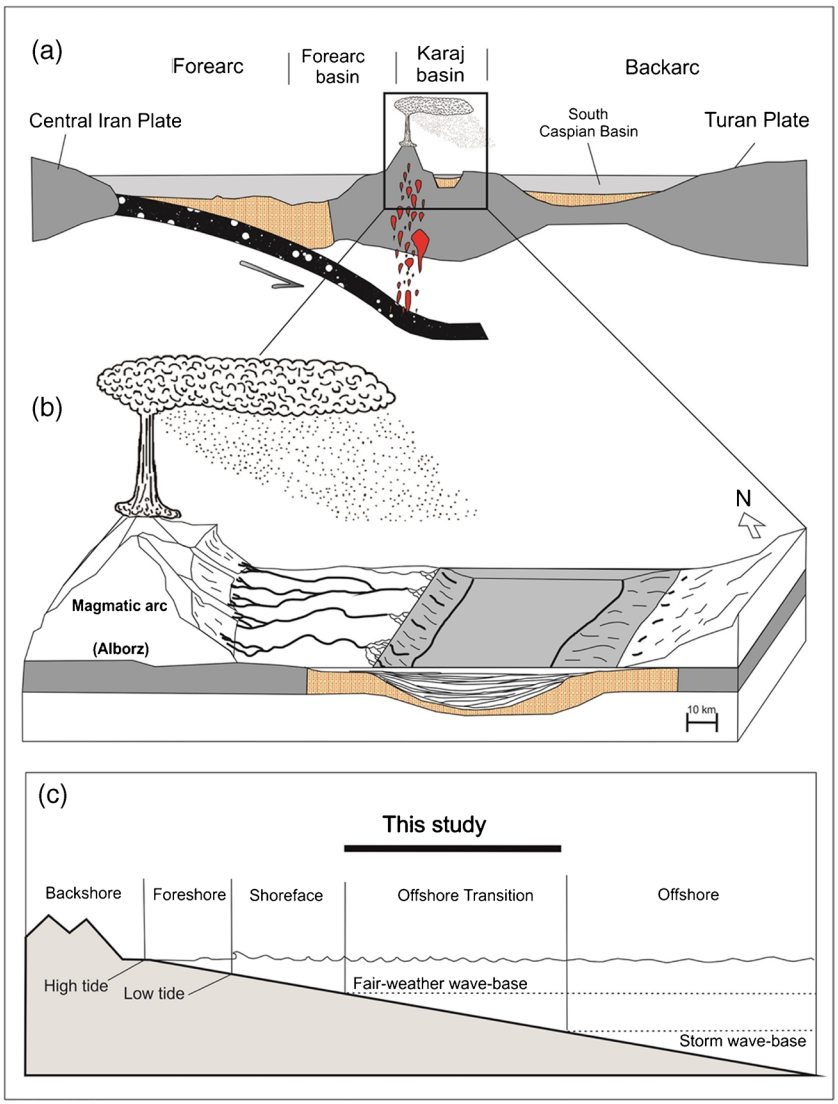

Fig. 12 **a** Tectonic setting of central Alborz during the Eocene. **b** Model suggesting the depositional environment of Asara Shale from Karaj Formation, Eocene, Iran. **c** Schematic diagram showing the bathymetric and temporal range of shallow marine depositional environments interpreted in this paper (Modified after Malekzadeh et al. 2020)

In summary, due to the oxygen-rich nature of the sedimentary environment and the presence of hyperpycnal flows associated with flood events, the Asara Shale environment is interpreted as accumulated in a shallow marine environment associated with hyperpycnal flows. The inferred environmental situation during the deposition of the Asara shale of the Karaj Formation is reconstructed in Fig. 12c.

Conclusions

The analysis of the sedimentological properties and depositional environments of the Asara Shale of Karaj Formation of the Alborz Basin of northern Iran suggest the following:

1. Shallow marine hyperpycnites were recognized in the Alborz Basin based on the description and interpretation of mainly suspended-load (Facies S) deposits. Evidence includes basal erosional surfaces, typical sedimentary structures related to an accumulation from sediment-laden turbulent flows, existence of plant remains related to terrestrial flood events, and the normal and inverse-then-normal-grading cycles related to waxing and then waning period of turbulent flow discharges.
2. A depositional model of shallow marine hyperpycnal flows was proposed in this study, shallow marine environment associated with hyperpycnal flows (offshore transition to shoreface).
3. The study of hydrocarbon generation potential in each region requires a detailed analysis of the existence of possible source rocks of that region. Source rocks are one of the most critical elements of the petroleum system. Therefore, to identify a hydrocarbon system in an area, it is necessary first to examine its origin and characteristics. Based on some factors such as the presence of hyperpycnal flows (a powerful mechanism of sedi-

ment supply), an oxidizing environment, and a lack of significant organic matter, it is considered that the Asara Shale in this area is not a potential source of hydrocarbons for future explorations. Indeed, this study is the first clear statement about the hydrocarbon potential of the Asara Shale as a member of the Karaj Formation.

Acknowledgements The authors would like to thank S. Ghadeer (Teshrin University) for his constructive comments and suggestions.

Data availability The authors confirm that the data supporting the findings of this study are available within the article (and/or) its supplementary materials.

Declarations

Conflict of interest The authors declare no competing interests.

References

Abbassi N, Lockley MG (2004) Eocene bird and mammal tracks from the Karaj Formation, Tarom Mountains, and northwestern Iran. Ichnos 11(3–4):349–356

Alimi N, Sajjadi F, Partouazar H (2010) Biostratigraphy and paleoenvironment of the Karaj Formation at the Chehel-Dokhtar section, north of Shahrood. Iran J Geol 4:3–21

Allen MB, Ghassemi MR, Shahrabi M, Qorashi M (2003) Accommodation of late Cenozoic oblique shortening in the Alborz range, northern Iran. Struct Geol 25:659–672

Amini A, Bolourian GHH (2005) Ash turbidite and submarine fans in Karaj Formation. Geosciences 14(55):146–153

Ataabadi MM, William S (2000) Eocene mammal footprints from Eastern Iran: a preliminary study. C R Acad Sci Ser II A 331:543–547. https://doi.org/10.1016/S1251-8050(00)01449-X

Ashley GM, Southard JB, Boothroyd JC (1982) Deposition of climbing-ripple beds: a flume simulation. Sedimentology 29(1):67e79. https://doi.org/10.1111/j.1365-3091.1982.tb01709.x

Asiabanha A, Foden J (2012) Post-collisional transition from an extensional volcano-sedimentary basin to a continental arc in the Alborz Ranges, N-Iran. Lithos 148:98–111

Birgenheier LP, Norton B, McCauley AD, Johnson CL, Kennedy A (2017) A depositional model for offshore deposits of the lower Blue Gate Member, Mancos Shale, Uinta Basin, Utah, USA. Sedimentology 64:1402–1438

Bolourian Gh (1992) Petrographic and petrological study of Karaj formation in Central Alborz. Master Dissertation, Teacher Training University

Buatois LA, Mangano MG (2011) Ichnology Compound trace fossils formed by plant and animal interactions: Quaternary of northern New Zealand and Sapelo Island, Georgia (USA). Fossils Strata 51:88–105

Dedual E (1967) Zur Geologie des mittleren and unteren Karaj-Tales, Zentral-Elburz (Iran). Zuerich, University, Geology. Inst Eidgenoess Tech Hochsh, Hochsh Inst, m Mitt 76:1–123

Dou L, Hou1 J, Song S, Zhang L, Liu Y, Sun S, Li Y, Wang X, Ren X, Tang Y, Tian H, YangY (2019) Sedimentary characteristics of hyperpycnites in a shallow lacustrine environment: a case study from the Lower Cretaceous Xiguayuan Formation, Luanping Basin, Northeast China. Geol J 1-17. https://doi.org/10.1002/gj.3599

Eriksson PG, Sarkar S, Samanta P et al (2010) Paleoenvironmental context of microbial mat-related structures in siliciclastic rocks. Microb Mats: Modern Ancient Microorganisms Stratified Syst 71–108. https://doi.org/10.1007/978-90-481-3799-2_5

Gallart F, Solé A, Puigdefábregas J & Lázaro R (2002) Scale-dependency of sediment yield from badland areas in Mediterranean environments. In: Bull LJ, Kirkby MJ (eds) Dryland rivers: hydrology and geomorphology of semi-arid channels, pp 299–326

Haaland HJ, Furnes H, Martinsen OJ (2000) Paleogene tuffaceous intervals, Grane Field (Block 25/11), Norwegian North Sea: Their depositional, petrographical, geochemical character and regional implications. Mar Pet Geol 17(1):101–118

Hagadorn JW, Bottjer DJ (1997) Wrinkle structures: microbially mediated sedimentary structures common in subtidal siliciclastic settings at the Proterozoic-Phanerozoic transition. Geology 25:1047–1050

Hickman-Lewis K, Westall F, & Cavalazzi B (2019) Traces of Early Life From the Barberton Greenstone Belt, South Africa, Earth's Oldest Rocks (Second Edition), Elsevier, 1029–1058, https://doi.org/10.1016/B978-0-444-63901-1.00042-3.

Jones B, Manning DAC (1994) Comparison of geochemical indices used for the interpretation of palaeoredox conditions in ancient mudstones. Chem Geol 111:111–129

Lasemi Y (2001) Facies analysis, depositional environments and sequence stratigraphy of the upper Pre-Cambrian and Paleozoic Rocks of Iran (in Persian). Geological Survey of Iran, Tehran, p 180

Lash GG (2016) Hyperpycnal transport of carbonaceous sediment — example from the upper Devonian Rhinestreet shale, western New York, USA. Palaeogeogr, Palaeoclimatol, Palaeoecol 459:29–43. https://doi.org/10.1016/j.palaeo.2016.06.035

Long DGF (2017) Evidence of flash floods in Precambrian gravel dominated ephemeral river deposits. Sediment Geol 347:53–66. https://doi.org/10.1016/j.sedgeo.2016.11.006

Maleki A, Saberi MH, Moallemi SA et al (2021) Evaluation of hydrocarbon generation potential of source rock using two-dimensional modeling of sedimentary basin: a case study in North Dezful Embayment, Southwest Iran. J Pet Explor Prod Technol 11:2861–2876. https://doi.org/10.1007/s13202-021-01202-5

Malekzadeh M (2016) Petrology and depositional environment of asara shale of Karaj formation in Kuh-e- Kond Section (North Eastern of Tehran). Master Dissertation, Shahid Beheshti University

Malekzadeh M, Wetzel A (2020) Paleodictyon in shallow-marine settings – an evaluation based on Eocene examples from Iran. Palaios 35(9):377–390. https://doi.org/10.2110/palo.2020.030

Malekzadeh M, Hosseini-Barzi M, Sadeghi A, Critelli S (2020) Geochemistry of Asara Shale member of Karaj Formation, Central Alborz, Iran: provenance, source weathering and tectonic setting. Marine Pet Geol 121:104584. https://doi.org/10.1016/j.marpetgeo.2020.104584

McKay JL, Pedersen TF, Mucci A (2007) Sedimentary redox conditions in continental margin sediments (N.E. Pacific) — influence on the accumulation of redox-sensitive trace metals. Chem Geol 238:180–196

Middleton GV (1965) Primary sedimentary structures and their hydrodynamic interpretation. https://api.semanticscholar.org/CorpusID:113492815

Miller W (2007) Trace fossils: concepts, problems, prospects. Geology Department Humboldt State University Arcata, CA, USA, p 637p

Modarres MH, Adabi M, Fayazi F, Behdad A, Moradpour M (2018) Petrography and geochemical composition of the middle Eocene, the Shahabazan Formation at Kialu Section, Zagros Basin, Southwestern Iran. Carbonates Evaporites 34. https://doi.org/10.1007/s13146-018-0438-x

Morley CK, Kongwung B, Julapour AA, Abdolghafourian M, Hajian M, Waples D, Warren JK, Otterdoom H, Srisuriyon K, Kazemi

H (2009) Structural development of a major late Cenozoic basin and transpressional belt in central Iran: the Central Basin in the Qom-Saveh area. Geosphere 5:325–362. https://doi.org/10.1130/GES00223.1
Morris RC (1971) Classification and interpretation of disturbed bedding types in Jackfork Flysch rocks (Upper Mississippian), Ouachita Mountains, Arkansas. J Sediment Petrol 41:410–424
Morton RA, Gelfenbaum G, Jaffe BE (2007) Physical criteria for distinguishing sandy tsunami and storm deposits using modern examples. Sediment Geol 200:184–207
Mulder T, Syvitski JPM, Migeon S, Faugères JC, Savoye B (2003) Marine hyperpycnal flows: initiation, behavior and related deposits, a review. Marine Pet Geol 20(6):861–882. https://doi.org/10.1016/j.marpetgeo.2003.01.003
Nadal-Romero E, Martínez-Murillo JF, Kuhn NK (Eds.) (2018) Badland Dynamics in the Context of Global Change. Elsevier, Amsterdam 320, Elsevier
Nazari EM, Syvitski JPM, Migeon S, Faugères JC, Savoye M (2003) Comparisons of fecundity, egg size, and egg mass volume of the freshwater prawns *Macrobrachium potiuna* and *Macrobrachium olfersi* (Decapoda, Palaemonidae). Crustac Biol 23(4):862–868
Nazari H (2000) Tectono magmatic and tectono stratigraphy of alborz magmatic arc, 18th Symposium of Geosciences, GSI
Noffke N (2009) The criteria for the biogenicity of microbially induced sedimentary structures (MISS) in Archean and younger, sandy deposits. Earth-Sci Rev 96:173–80
Noffke N (2010) Microbial Mats in Sandy Deposits from the Archean Era to Today. Springer, New York, Springer
O'Brian NR, Slatt RM (1990) Argillaceous Rock Atlas. Springer-Verlag, New York, Springer-Verlag
Petter AL, Steel RJ (2006) Hyperpycnal flow variability and slope organization on an Eocene shelf margin, central basin, Spitsbergen. AAPG Bull 90(10):1451–1472. https://doi.org/10.1306/04240605144
Plink-Björklund P, Steel RJ (2004) Initiation of turbidity currents: outcrop evidence for Eocene hyperpycnal flow turbidites. Sediment Geol 165(1):29–52. https://doi.org/10.1016/j.sedgeo.2003.10.013
Rezaeian M (2008) Coupled tectonics, erosion and climate in the Alborz Mountains, Iran. PhD Dissertation thesis, University of Cambridge
Shahidi A, Barrier E, Brunet MF, Saidi A (2011) Tectonic evolution of the Alborz in Mesozoic and Cenozoic. Scientific Quarterly Journal, Geosciences, p 21
Solanki PM, Bhatt NY, Patel SJ (2015) Lithofacies and ichnology of Jumara Formation of Bharasar Dome, Kachchh, Western India. J Geosci Res 1:29–43
Steel E, Simms AR, Steel R, Olariu C (2018) Hyperpycnal delivery of sand to the continental shelf: insights from the Jurassic Lajas Formation, Neuquén Basin, Argentina. Sedimentology 65:2149–2170
Sumner EJ, Amy LA, Talling PJ (2008) Deposit structure and processes of sand deposition from decelerating sediment suspensions. J Sediment Res 78(8):529–547
Vahdati Daneshmand F (1997) Quadrangle Geological map of the East of Tehran, scale 1:100,000. Geological Survey of Iran. Tehran, Iran
Walker RT, Fattahi M (2011) A framework of Holocene and Late Pleistocene environmental change in eastern Iran inferred from the dating of periods of alluvial fan abandonment, river terracing, and lake deposition. Quatern Sci Rev 30(9–10):1256–1271. https://doi.org/10.1016/j.quascirev.2011.03.004
Wignall PB (1994) Black shales. Clarendon Press, Oxford
Wignall PB, Twitchett RJ (1996) Oceanic anoxia and the end Permian mass extinction. Science 272:1155–1158
Xian B, Wang J, Gong C, Yin Y, Chao C, Liu J, Yan Q (2018) Classification and sedimentary characteristics of lacustrine hyperpycnal channels: Triassic outcrops in the south Ordos Basin, central China. Sed Geol 368:68–82. https://doi.org/10.1016/j.sedgeo.2018.03.006
Xing ZF (2010) Study on microbially induced sedimentary structures (MISS) from the Mesoproterozoic Yunmengshan formation in Western Henan Province. Unpublished Master Dissertation, Henan Polytechnic University
Yoshida M, Yoshiuchi Y, Hoyanagi K (2010) Occurrence conditions of hyperpycnal flows, and their significance for organic-matter sedimentation in a Holocene estuary, Niigata Plain, Central Japan. Island Arc 18(2):320–332
Yu T, Enjie H, Hongde C.H, Hehua W, Wei H, Hao Y, Yijiu Z, Shicheng L (2018) Petrology, lithofacies, and sedimentary environment of Upper Cretaceous Abu Roash "G" in the AESW Block, Abu Gharadig Basin, Western Desert, Egypt. Afr Earth Sci 178–189. https://doi.org/10.1016/j.jafrearsci.2018.05.017
Zavala C (2020) Hyperpycnal (over density) flows and deposits. J Palaeogeogr 9:17. https://doi.org/10.1186/s42501-020-00065-x
Zavala C, Pan SX (2018) Hyperpycnal flows and hyperpycnites: origin and distinctive characteristics. Lithologic Reserv 30(1):1–27
Zavala C, Arcuri M, Valiente LB (2012) The importance of plant remains as diagnostic criteria for the recognition of ancient hyperpycnites. Rev Paléobiol 11(6):457–446
Zavala C, Arcuri M, Di Meglio M, Zorzano A, Otharán G, Irastorza A, Torresi A (2021) Deltas: A new classification expanding Bates's concepts. J Palaeogeogr 10(3):341–355. https://doi.org/10.1186/s42501-021-00098-w
Zavala C, Arcuri M, Gamero H et al (2011) A genetic facies tract for the analysis of sustained hyperpycnal flow deposits. https://doi.org/10.1306/13271349St613438
Zavala C, Ponce JJ, Arcuri M, Drittanti D, Freije H, Asensio M (2006) Ancient lacustrine hyperpycnites: a depositional model from a case study in the Rayoso Formation (Cretaceous) of west-central Argentina. Sediment Res 76(1–2):41–59. https://doi.org/10.2110/jsr.2006.12
Zheng W, Qi YA, Xing ZF, Bai WB, Chen BB, Li XY (2017) Characteristic and paleoenvironment significance of microbially induced sedimentary structures (MISS) in continental P-T boundary in Jiyuan, Western Henan Province. Acta Sedimentol Sin 35:1121–1132 (in Chinese with English abstract)